




Article

Cleaning Schedule Optimization of Heat Exchangers with Fouling on Tube and Shell Sides: A Metaheuristic Approach

João P. V. de Cesaro ^{1,2}, Mauro A. S. S. Ravagnani ¹, Fernando D. Mele ² and Caliane B. B. Costa ^{1,*}

¹ Chemical Engineering Graduate Program, State University of Maringá, Avenida Colombo 5790, Maringá 87020900, Brazil; pg55952@uem.br (J.P.V.d.C.); massravagnani@uem.br (M.A.S.S.R.)

² Department of Process Engineering and Industrial Management, Universidad Nacional de Tucumán, Av. Independencia 1800, San Miguel de Tucumán T4002LBR, Argentina; fmele@herrera.unt.edu.ar

* Correspondence: cbbcosta@uem.br

Abstract: Pre-heat trains (PHTs) significantly reduce refinery fuel consumption and carbon emissions. However, these benefits are diminished by fouling in heat exchangers (HEXs). Current methods for optimizing cleaning schedules often report high computation times due to the transient nature of the fouling process and do not consider shell-side fouling, which can be significant for some oil fractions. This paper addresses these issues by adding shell-side fouling to the model and by transforming cleaning time variables into integers, reducing the problem of optimizing cleaning schedules to an integer nonlinear programming (INLP) problem. The reformulated problem is solved using integer particle swarm optimization (PSO) coupled with a simple search strategy, where the number of cleaning actions is preset and their timing is optimized. The adopted approach achieved up to 84% lower computation times compared to previous ones. Additionally, the relationship between cleaning actions and PHT performance is nonlinear, with diminishing returns from additional cleaning, and optimal cleaning schedules are often asymmetric for different HEXs within the same PHT. The proposed approach effectively reduces operating costs and provides a framework for future optimization enhancements.



Academic Editors: Tadeusz Bohdal and Marcin Kruzel

Received: 11 December 2024

Revised: 23 December 2024

Accepted: 25 December 2024

Published: 28 December 2024

Citation: de Cesaro, J.P.V.; Ravagnani, M.A.S.S.; Mele, F.D.; Costa, C.B.B. Cleaning Schedule Optimization of Heat Exchangers with Fouling on Tube and Shell Sides: A Metaheuristic Approach. *Energies* **2025**, *18*, 71. <https://doi.org/10.3390/en18010071>

Copyright: © 2024 by the authors. Licensee MDPI, Basel, Switzerland. This article is an open access article distributed under the terms and conditions of the Creative Commons Attribution (CC BY) license (<https://creativecommons.org/licenses/by/4.0/>).

Keywords: heat exchanger; particle swarm optimization; fouling; aging; scheduling

1. Introduction

Pre-heat trains in refineries play a crucial role in reducing fuel consumption and lowering carbon emissions by improving energy use. However, these gains are diminished by the occurrence of fouling in the heat exchangers (HEXs) of the pre-heat trains. Fouling costs are estimated to be around USD 1–1.2 billion per year in the US alone, leading to 2.2 million tons of extra carbon dioxide emitted [1]. Given the urgent global need to reduce greenhouse gas emissions and improve energy efficiency, the effective management of fouling and its aging process in heat exchanger networks (HENs) is critical to ensuring the sustainability of industrial energy systems.

After fouling occurs, the fouled particles, which have ‘gel-like’ characteristics, may react into ‘coke-like’ particles. This process is known as aging and it occurs at higher temperatures due to the higher activation energy that is required. The aged particles have higher thermal conductivity and their presence usually comes with greater pressure drops within a HEX [2]. These particles are also harder to remove and demand more physical cleaning actions [3], which are costlier and longer-lasting [4].

Coletti et al. [5] highlighted the detrimental effects of fouling on carbon emissions. They underscored the substantial contribution of emissions to costs, amounting to over

USD 1.3 million annually. Abdulhussein et al. [6] examined water samples before and after cleaning actions, revealing significant increases in oil and sulfide content post washing, leading to environmental contamination. Ishiyama et al. [1] discussed the operational and environmental implications of fouling, noting a decline in refinery numbers in the US alongside a reduction in fouling-induced emissions, despite an increase in oil processing volume.

The Ebert–Panchal equation [7] has been widely adopted for fouling estimations over the past two decades, while aging and shell-side fouling models have seen ongoing development. Ishiyama et al. [8] introduced a lumped parameter system demonstrating aging's influence on heat transfer and fouling rates, emphasizing its importance in interpreting experimental data and heat exchanger modeling. Coletti et al. [9] expanded on this by studying the effects of roughness on fouling rates, focusing on single-tube analyses to enhance accuracy. Coletti et al. [10] compared distributed model results to refinery data, revealing excellent agreement with the measured plant data. The authors concluded the current model was limited by the lack of pressure drop measurements when considering HEXs with significant shell-side fouling. Ishiyama et al. [11] proposed a simplified two-layer model, showing good agreement with distributed models, especially in systems with constant heat flux. Ishiyama et al. [12] explored the impact of aging on cleaning actions, concluding that mechanical methods are essential for aged particles. Ishiyama et al. [4] monitored temperature and pressure drops, emphasizing the importance of accurate surface roughness values. They highlighted that aging alters deposit thickness, affecting fouling formation rates. Furthermore, monitoring pressure drops aids in understanding changes in hydraulics and convective coefficients, crucial for accurate modeling [13].

Recent efforts have also improved the understanding and estimation of shell-side fouling, with Loyola-Fuentes et al. [14] employing data reconciliation to estimate shell-side fouling and Diaz-Bejarano et al. [15] updating equations for the Bell–Delaware model and adjusting threshold fouling models to estimate shell-side fouling.

Although fouling in refinery pre-heat trains is the focus of this work, it is also a concern in other industries such as milk [16,17], syngas [18], desalinated water [19], and phosphoric acid [20] production. Several strategies may be used to mitigate fouling. These may be put into two categories: preventive and remedial. In the preventive category, there is the usage of antifoulants and different blends, improving heat exchanger designs by, for instance, smoothing surfaces or inserting turbulence promoters [21], adding a coating to avoid reactions with heat exchanger materials [22], and controlling mass flow rate distribution in parallel configurations [23]. In the remedial category, there is the use of proportional–integral–derivative controllers [24] and, the most used method, cleaning heat exchangers in conjunction with cleaning scheduling optimization or heuristics.

Rogel et al. [25] studied the effect of different oil blends on fouling rates and concluded that asphaltene and ash contents have a minor contribution. Their study shows that the blend of highly paraffinic crude oils with medium and heavy ones decreases asphaltene solubility, which greatly contributes to fouling. The authors observed that, although correlations based on asphaltene and ash contents described fouling effects well for the first hour of the experiment, this did not hold true for longer times, as blend compatibility became more important [26]. Additionally, Obaidi and collaborators [27] tested fouling rates with different antifoulant concentrations and concluded that it yielded the best results at lower concentrations (35 ppm). M'barki et al. [28] evaluated the effects of paraffin inhibitors on crude oil and found that the ability of asphaltenes to function as paraffin inhibitors is related to oil complexity. Villardi et al. [29] found that mixing the tested blends led to much higher fouling rates, which were attributed to thermodynamic imbalances due to mixing.

HEX design optimization has been studied by using threshold fouling modeling and minimizing the heat exchanger area while trying to keep fouling to a minimum in the work of Lemos et al. [30]. The work has been further elaborated by adding shell-side fouling into the model and considering the hydraulic effects of fouling on the HEX. The main benefit of considering fouling in the design is that it can identify solutions with a considerable reduction in total areas, as the solver tries to mitigate fouling effects [31]. Research has also been carried out on the subject of retrofitting HENs with fouling, leading to larger periods between cleaning actions [32].

The optimization of the flow rate has been studied both for different initial fouling widths and for different HEX designs. Assis et al. [23] studied the flow rate distribution for both tube and shell sides and found that the average furnace duty decreased from 5149 to 4801 kW by their approach. Carvalho et al. [33] parametrized the flow rate distribution while considering fouling on both sides, obtaining a USD 46,000.00 reduction in costs. Lozano-Santamaria and Macchietto [34] optimized both cleaning scheduling and shell-side flow rate distribution for pressure-driven HENs and obtained 25% further savings compared to considering cleaning scheduling alone.

Research on optimizing heat exchanger cleaning schedules has been explored through various approaches. Ishiyama et al. [35] used a “greedy” algorithm to analyze fouling mitigation options, which included combined cleaning and antifoulant usage. Pogiatis et al. [36] utilized a nonlinear programming (NLP) approach to determine the number of chemical cleanings between mechanical cleaning actions, demonstrating its superiority over heuristics in identifying optimal schedules. Assis et al. [37] proposed a mixed integer nonlinear programming (MINLP) approach, significantly reducing costs compared to heuristic methods. Diaby et al. [38,39] investigated the impact of aging on cleaning schedules and then employed genetic algorithms for optimization. Al Ismaili et al. [40] framed the problem as a mixed-integer multistage optimal control problem, observing distinct bang-bang behavior. Lozano-Santamaria and Macchietto [34] introduced complementary constraints to enhance computational efficiency in optimizing cleaning schedules for HENs. Elwerfalli et al. [41] proposed a risk-based inspection approach, recommending a frequency of at least one shutdown every 600 days for the studied HEX. Lastly, Trafczynski et al. (2023) [42] applied a measurement-aided monitoring method, detailed earlier by the same research group [43], and simplified the problem to integer nonlinear programming (INLP) to improve computational tractability. These studies collectively contribute diverse insights and approaches to the optimization of heat exchanger cleaning schedules.

Although important, tube-side aging and, especially, shell-side fouling are still ignored in some papers as they are not as well-understood phenomena as tube-side fouling. Ignoring aging may lead to lower total fouling widths and an overestimation of total fouling resistances, as the threshold models used are inversely related to the HEX tube side’s Reynolds number. On the other hand, not adding shell-side fouling leads to a smaller total resistance [14].

Another aspect that could be improved is the computation time required for performing the optimization tasks. For instance, optimizing a small HEN consisting of two one-shell heat exchangers in series can demand over 484 CPU seconds using an “Intel Core i7 computer, 3.40 GHz, 16.0 GB RAM” [34]. Consequently, it would be extremely challenging to incorporate additional levels to the optimization, such as optimizing HEX design and cleaning scheduling simultaneously or performing HEN synthesis, in which the cleaning scheduling optimization code might need to be run hundreds of thousands of times.

Although prior research has extensively explored fouling and aging in heat exchangers, this work presents a novel approach by simultaneously considering fouling on both sides

of the HEX and aging exclusively on the tube side in cleaning schedule optimization. The introduction of an integer particle swarm optimization (PSO) method to solve the INLP problem offers a new and efficient approach to the cleaning scheduling optimization problem. Unlike traditional MINLP approaches, which often face high computational costs, this method reduces simulation times while maintaining accuracy. Additionally, this study addresses computational challenges such as natural loops, related to variables that must be estimated through iterative methods, which have been underexplored in previous optimization efforts.

2. Methods

This section discusses the methods used in this work. Section 2.1 explains the problem statement. Section 2.2 discusses the solution approach we used. Section 2.3 presents the models used to simulate the heat exchangers.

The programming logic and further information on the methods used to solve pressure-driven flow distribution estimation, countercurrent flow temperature estimation, resistance rates ordinary differential equations (ODEs), and the optimization of the cleaning problem are available in Supplementary Material File S1.

2.1. Problem Statement

This study models and simulates HENs experiencing fouling phenomena. The network is used to heat crude oil in refinery pre-heat trains (PHTs) before it proceeds to a distillation column, and all HEXs presently operate in crossflow. After passing through the HEN, the crude oil is further heated in a furnace to reach the distillation column's target inlet temperature. This study's focus is to determine the optimal cleaning schedule policy over a year of operation to minimize the total costs associated with heating crude oil and HEN maintenance.

As fouling occurs and progresses, the HEN's pressure drop increases and its heat exchange efficiency decreases over time. This results in higher pumping power requirements and greater furnace loads, leading to increased fuel consumption and carbon dioxide emissions. Cleaning actions remove the accumulated fouling, but they also incur costs and temporarily increase furnace loads during the cleaning process. The objective function to be minimized includes the total costs associated with the crude oil heating operation, such as fuel oil prices, carbon emission credits, cleaning action expenses, and electricity costs for the pumping power needed to compensate for the HEN's pressure drops. The minimization of the objective function is achieved through the adjustment of the cleaning periods of each HEX. Furthermore, the HEN topology, HEX designs, and the number of cleaning actions for each HEX are known parameters in the optimization.

2.2. Solution Approach

The hypotheses used for all studied systems are (i) adiabatic operation in relation to the surroundings; (ii) a pseudo-stationary state for ten-day intervals, as the rate of heat transfer is much higher than deposition rates; (iii) heat transfer and deposition happen in a radial direction only; (iv) the mass flow rates of fluids are constant, although they vary for each heat exchanger when in parallel; (v) constant fluid characteristics; (vi) fouling and aging rates are uniform throughout each HEX's shell; and (vii) when a cleaning action takes place, the HEX is bypassed (this means not all heat exchangers in a line need to be stopped at once).

As the system is in transient operation, the pseudo-stationary hypothesis is made, as this approach lowers modeling complexity while not affecting accuracy [14]. The considered operation period is one year, and this period is divided into thirty-seven ten-day

intervals, spanning from 0 (initial conditions) to 370. This means that HEX variables and resistances are calculated up to the 360th day and aggregated and monetary calculations (explained in Section 2.3.6) take up to the 370th into account, due to the pseudo-stationary assumption. The decision variables (times in which cleaning actions are carried out) are discretized to solve the fouling resistance ODEs, thereby transforming the MINLP into an INLP.

The objective function (OF) is represented in Equation (1).

$$OF = n_{seconds} \cdot \sum_{p=0}^{N_{per}} \left(C_{fuel} + C_{CO_2} + \left[\sum_{HEX=0}^{N_{HEX}} C_{pumping} + C_{cleaning} \right] \right) \quad (1)$$

In Equation (1), N_{per} is the number of periods considered, $n_{seconds}$ is the number of seconds in the ten-day period, C_{fuel} stands for the costs associated with fuel usage in each period, C_{CO_2} is the price associated with carbon emission in each period, $C_{pumping}$ is the additional price of pumping for each HEX in each period, and $C_{cleaning}$ is the price associated with cleaning each HEX in each period, which is equivalent to the price of one cleaning action, if a cleaning action occurs for the considered HEX and period, and zero otherwise.

Given the HEN topology, the initial resistance values, and the number of cleaning actions that are set to each HEX, the decision variables considered in the optimization are the periods in which each cleaning action (associated with a specific HEX) takes place. Naturally, the periods are integer values from 0 to 36. However, period thirty-two was set as the upper bound for the decision variables. The bound was set so because cleaning actions in the last few periods do not occur, as other operating costs do not have enough time to offset costs associated with the cleaning action.

The system is constrained by an upper limit for the furnace duty (equal to 50 MW). However, this limit was addressed through a penalization factor (one percent of the objective function value is added for each 1 MW unit over the upper limit), since reducing the production capacity of the refinery far outweighs any other costs related to the PHT [5].

2.3. Modeling

This section presents the modeling used for the simulation of the heat exchangers. The equations presented were kept roughly in the order they are calculated in the source code, as this makes reimplementation easier. One exception is the fouling equations, as they are calculated after temperature estimations.

2.3.1. Bell–Delaware Equations

The heat exchangers were modeled using Bell–Delaware equations [44]. Some parameters must be arbitrated so correction factors and shell-side convective coefficients can be calculated. However, the parameters that are set may change from work to work. In this work, the set parameters are as follows: (i) tube outer diameter, $2r_o = d_o$ (mm); (ii) tube inner diameter, $2r_i^{clean} = d_i^{clean}$ (mm); (iii) wall conductivity, k_w ($\text{W} \cdot \text{m}^{-1} \cdot \text{K}^{-1}$); (iv) shell diameter, $2r_s = D_s$ (m); (v) number of tubes, N_t ; (vi) number of tube passes, N_p^{tube} ; (vii) number of shell passes, N_p^{shell} ; (viii) effective tube length, L_t (m); (ix) baffle cut, B_c (%); (x) baffle spacing, L_{bc} (m); and (xi) tube layout. With those parameters set, all others may be calculated. As the difference in the outer radius resulting from shell-side fouling was not considered, due to it being much smaller than tube-side fouling, most of these calculated parameters are constant. The only exceptions are variables dependent on the shell-side mass flow rate.

2.3.2. Fouling Equations

The shell-side convective coefficient was estimated using a constant fouling rate (α_2) [14]. The models used to estimate tube-side fouling resistances were the modified Ebert–Panchal and first-order kinetic models taken from Coletti et al. [9] and Diaz-Bejarano et al. [15], respectively. The fouling models used in this study are well established in the literature and have undergone extensive validation by their original authors through experimental and industrial data [7,11,12,14]. Those are given by Equations (2) and (3).

$$\frac{dR_{f,g}}{dt} = \alpha_1 Pr^{-0.33} Re^{-0.66} \exp\left(-\frac{E_f}{RT_f}\right) - \gamma \tau_w \quad (2)$$

$$\frac{dR_{f,c}}{dt} = \frac{A_a}{\lambda_c} \exp\left(-\frac{E_a}{RT_{gc}}\right) \delta_g \quad (3)$$

In Equations (2) and (3), $R_{f,g}$ and $R_{f,c}$ are gel and coke resistances, respectively. α_1 is the deposition coefficient, A_a is the pre-exponential aging factor, λ_c is the coke's thermal conductivity, Pr and Re are the Prandtl and Reynolds numbers, E_f and E_a are fouling and aging activation energies, T_f and T_{gc} are the film and gel–coke interface temperatures, R is the universal gas constant, γ is the suppression coefficient, and τ_w is the shear stress.

With the formation of fouling layers, the tube-side radius varies with time. Therefore, their widths must be estimated to update the radius for each period. They are calculated through Equations (4)–(7) [45]. On the other hand, tube outer radii are considered constant, as shell-side fouling rates are much smaller than the ones on the tube side and there are no aging phenomena (which lead to considerably higher fouling widths).

$$\delta_c = r_i^{clean} \left[1 - \exp\left(-\frac{\lambda_c R_{f,c}}{r_o}\right) \right] \quad (4)$$

$$\delta_g = (r_i^{clean} - \delta_c) \left[1 - \exp\left(-\frac{\lambda_g R_{f,g}}{r_o}\right) \right] \quad (5)$$

$$\delta_{tube} = \delta_c + \delta_g \quad (6)$$

$$r_i(t) = r_i^{clean} - \delta_{tube} \quad (7)$$

In Equations (4)–(7), δ_c , δ_g , and δ_{tube} are the coke, gel, and total tube fouling width, respectively. λ_c and λ_g are the coke and gel thermal conductivity coefficients. $r_i(t)$ represents the current tube radius. The gel fouling width equation discounts coke width in its calculations. The total fouling thermal resistance R_f is then calculated using Equation (8).

$$R_f = \frac{1}{\lambda_g} \delta_g + \frac{1}{\lambda_c} \delta_c \quad (8)$$

2.3.3. Hydraulic Variables

The friction factor (ff) is calculated through the Serghides equation given by Of- for and Alibi [46] and shown in Equations (9)–(12). This equation is used for turbulent flow ($Re > 2100$). S_1 , S_2 , and S_3 are repeating parameters that are used to estimate the friction factor.

$$S_1 = -2\log(rug/3.7 + 12/Re) \quad (9)$$

$$S_2 = -2\log(rug/3.7 + 2.51 \cdot S_1/Re) \quad (10)$$

$$S_3 = -2\log(rug/3.7 + 2.51 \cdot S_2/Re) \quad (11)$$

$$ff = \left[S_1 - \frac{(S_2 - S_1)^2}{S_3 - 2S_2 + S_1} \right]^{-2} \quad (12)$$

Mass flux and pressure drop are calculated through Equations (13) and (14), respectively, where ρ is the fluid's density [45].

$$G_t = \frac{m}{\pi r_i^2(t)} \frac{N_p^{tube}}{N_t} \quad (13)$$

$$\Delta P = \frac{G_t^2}{2\rho} \left[\frac{1.5}{N_p^{tube}} + \frac{ff \cdot L_t}{2r_i(t)} + 4 \right] N_p^{tube} \quad (14)$$

2.3.4. Convective Coefficients

The shell-side convective coefficient for ideal crossflow (h_s^i) is adjusted through correction factors that consider the several pathways shell-side fluids can take and their respective flow fractions (J), resulting in the shell-side heat transfer coefficient (h_s), calculated by Equations (15) and (16) [44].

$$h_s^i = \left(0.236 \cdot Re_s^{-0.346} \right) \cdot \left(\frac{C_{p_s} G_s}{Pr_s^{2/3}} \right) \quad (15)$$

$$h_s = h_s^i \cdot (J_c J_l J_b J_s J_r), \quad J_r = J_s = 1 \quad (16)$$

In Equation (16), C_{p_s} is the specific heat of the shell-side fluid, Pr_s is the shell-side Prandtl number, Re_s is the shell-side Reynolds number, and G_s is the shell-side mass flux. Although the method considers five types of correction factors, in this work, both J_r , the correction factor related to laminar flow ($Re < 100$), and J_s , the correction factor related to unequal baffling spacing, are not evaluated, as only heat exchangers well within a turbulent flow regime were analyzed and inlet and outlet spacing were considered equal to baffle spacing (L_{bc}) within the heat exchangers. The considered correction factors for the segmental baffle window (J_c), bundle bypass effects (J_b), and baffle leakage effects (J_l) are, respectively, related to the fraction of tubes in the baffle window, the bundle bypass area, and the tube-to-baffle-hole and shell-to-baffle leakages. The tube side convective coefficient (h_t) is calculated by Equation (17), where k is the fluid's conductivity.

$$h_t = \frac{k}{2 \cdot r_i(t)} \cdot 0.027 \cdot Re_t^{0.8} \cdot Pr_t^{1/3} \quad (17)$$

The overall heat transfer coefficient (U) is then calculated through the inverse of the aggregation of all resistances present in the heat exchanger.

$$U = \left[\frac{1}{h_s} + R_{f,s} + \frac{(r_o - r_i(t))}{k_w} \cdot \frac{r_o}{r_o + r_i(t)} + \frac{1}{h_t} \cdot \left(\frac{r_o}{r_i(t)} \right) + R_{f,t} \cdot \left(\frac{r_o}{r_i(t)} \right) \right]^{-1} \quad (18)$$

In Equation (18), $r_o/r_i(t)$ refers to a correction for tube side variables, k_w is the wall conductivity, $R_{f,s}$ is the total shell-side fouling resistance, and $R_{f,t}$ is the total tube-side fouling resistance.

2.3.5. Temperature Estimation

Outlet temperatures and heat loads are estimated using the effectiveness–number of transfer units (P-NTU) method. The equations of the method use the tube’s inner diameter as the reference point, as it is variable. Therefore, all equations use the tube-side fluid as its reference for calculations. This method uses the effectiveness of the heat exchanger, the capacity ratio between fluids, and the number of transfer units to estimate heat exchanger duty and outlet, average, film, fluid–gel interface, and gel–coke interface temperatures. The equations were taken from the work of Lozano-Santamaria and Macchietto [45].

For two shells in a countercurrent, an analytical solution for the P-NTU system of equations was obtained as a means of reducing computation times. More information on the equations and methods may be found in Supplementary Material File S1.

2.3.6. Aggregated and Monetary Calculations

The aggregated calculations represent the summation of parameters across all time periods or shells. Consequently, they are computed only once after simulating all periods, rather than for each period. Subsequently, the aggregated parameters are adjusted by multiplying them by the number of seconds in a ten-day period, when necessary, and then converted into appropriate units of measurement.

The furnace load (Q_{furn}) is calculated by Equation (19). The HEN is created in the code as a conjunction of nodes, such as entrances, outlets, splitters, mixers, and HEXs (further information is available in Supplementary Material File S1). Therefore, the coil inlet temperature (CIT) depends on the next node of the last heat exchanger, as heat exchanger indexes are organized from colder to hotter temperatures.

$$Q_{furn} = (COT - CIT) \cdot \frac{\dot{m}_{crude} \cdot C_p^{crude}}{\eta_{furn}} \quad (19)$$

In Equation (19), COT is the coil outlet temperature, or, in other words, the target temperature of the crude oil; \dot{m}_{crude} is the crude oil mass flow rate; C_p^{crude} is the specific heat capacity of crude oil; and η_{furn} is the furnace efficiency. Carbon emissions were calculated by multiplying the furnace load by a carbon-emission-to-fuel ratio.

Another parameter calculated at this level is the pumping power (Q_{pump}) required to compensate for pressure drops in heat exchangers, given by Equation (20), where η_{pump} is the pump effectiveness.

$$Q_{pump} = \frac{\dot{m}_{tube} \cdot \Delta P_{tube}}{\eta_{pump} \cdot C_p^{tube}} \quad (20)$$

Total costs are calculated by summing individual costs, such as fuel, carbon, cleaning, and pumping. These costs are calculated by multiplying the aggregated units by their unitary cost. As an example, the yearly energy consumption multiplied by the energy cost per megawatt-hour (MWh) gives the total energy cost.

3. Results and Discussion

This section is divided into case studies of different heat exchanger networks. The cases studied are described in Table 1.

The physical properties of the studied fluids were considered constant throughout this work, and they are given in Table 2 [34]. All remaining model and heat exchanger parameters were taken from Lozano-Santamaria and Macchietto [34] and are displayed in Table 3. The aging pre-exponential factor and activation energy used were 129.6 day^{-1} and 50 kJ mol^{-1} , respectively. The operational specifications for all case studies were 50 MW maximum furnace duty, 0.90 furnace efficiency, 0.70 pump efficiency, costs of USD

27 MWh^{−1} for fuel, USD 50 MWh^{−1} for electricity, USD 30 ton^{−1} for carbon emissions, USD 30,000 or cleaning action, a carbon emission to fuel ratio of 0.011 ton MWh^{−1}, and 10 days for a cleaning action to finish [34].

Table 1. Case studies' names and descriptions.

Name	Description
CS1	One heat exchanger
CS2	Two heat exchangers in parallel configuration
CS3	Two heat exchangers in countercurrent configuration
CS4	Four heat exchangers in parallel with two HEXs in countercurrent in each branch
CS5	Four heat exchangers in countercurrent

Table 2. Fluid average physical properties.

Fluid	Density (kg m ^{−3})	Thermal Conductivity (W m ^{−1} K ^{−1})	Specific Heat Capacity (J kg ^{−1} K ^{−1})	Viscosity (Pa s)
Crude oil	621.08	0.09	2846.42	2.716×10^{-4}
Vacuum residue (VR)	854.00	0.15	2555.00	7.215×10^{-5}
Light Gas Oil	710.66	0.11	2736.88	2.994×10^{-4}

Table 3. HEX and model parameters for Case Studies 1, 2, 3, 4, and 5 (CS1, CS2, CS3, CS4, and CS5, respectively).

	d_i^{clean} (mm)	d_o (mm)	L_t (m)	N_t	N_p^{tube}	k_w (W m ^{−1} K ^{−1})	D_s (m)	N_p^{shell}	α_2 (m ² ·K·kWh ^{−1})	α_1 (m ² ·K·W ^{−1} ·day ^{−1})	γ (m ⁴ ·K·N ^{−1} ·W ^{−1} ·day ^{−1})	E_f (kJ·mol ^{−1})
CS1, CS2, CS3	19.05	25.4	5.7	880	4	38	1.4	1	5.50×10^{-4}	142.56	8.04×10^{-8}	28.5
CS4	16.35	19.05	6.1	1032	4	38	0.94	1	5.50×10^{-4}	142.56	8.04×10^{-8}	28.5
CS5-HEX1/2	16.35	19.05	4.45	900	2	38	0.8475	1	0	142.56	0	28.5
CS5-HEX3/4	16.35	19.05	6.1	1810	4	38	1.296	1	0	142.56	8.04×10^{-8}	28.5

All calculations were performed on a Dell Inspiron 3583 computer with the following specifications: Intel(R) Core(TM) i7-8565U CPU @ 1.80 GHz (1.99 GHz), 16 GB of RAM, and a 64-bit operating system.

3.1. Case Study 1

Case Study 1 refers to the cleaning optimization of one heat exchanger. The tube-side fluid used was crude oil and the shell-side fluid was vacuum residue, which have mass flow rates of 88 and 26 kg s^{−1} and inlet temperatures of 483.15 and 603.15 K, respectively. All remaining model and heat exchanger parameters are displayed in Table 3. The only exceptions were the tube outer diameter, which was taken from Coletti and Macchietto [5], and the shell-side fouling rate, which was taken from Loyola-Fuentes et al. [14].

The first step was to vary the number of cleaning actions set for the heat exchanger. Table 4 displays the main results related to the HEX as cleaning actions are added to the process.

As seen in Table 4, the average time taken for the optimization was 4.85 s, of which an average of 3.68 s was taken estimating ODE values. In comparison with other work, Lozano-Santamaria and Macchietto [34] were able to solve the one-HEX problem in 3.57 s by limiting it to up to two cleaning actions and using a mathematical program with a complementarity constraint approach. The equivalent of this would take 9.7 s in the present formulation. However, the number of PSO iterations in this code is high (60 iterations), as it was kept constant for all case studies for the sake of comparison. When this value was

reduced to 15 maximum iterations, computation times were reduced to 1.65 s. Added to that, Lozano-Santamaria and Macchietto [34] used an “Intel Core i7 computer, 3.40 GHz, 16.0 GB RAM”, whilst the calculations for this work were carried out on a computer with a processor speed of 1.80 GHz and similar configurations otherwise.

Table 4. Computation times (CT), HEX duty, furnace energy, carbon footprint, total costs, and cleaning periods (CIPs) for Case Study 1.

Parameter	Unit	1 Action	2 Actions	3 Actions	4 Actions
Total CT	s	4.74	5.03	4.76	4.87
ODE CT	s	3.60	3.84	3.54	3.75
HEN duty	MWh	39,536.0	43,804.7	45,834.5	45,834.5
Furnace energy	MWh	343,718.3	338,975.3	336,720.0	336,720.0
Carbon emitted	ton	3780.9	3728.7	3703.9	3703.9
Total costs	USD	9,423,822	9,324,196	9,292,557	9,292,557
HEX1 CIPs	-	{18}	{12,25}	{9,19,28}	{9,19,28,28}

For Case Study 1, three cleaning actions yielded the best results with a cost of USD 9,292,557 for a year. This represents a reduction of USD 131,266 and USD 31,639 in relation to the cases with one and two cleaning actions.

For this case, with no interaction between different heat exchangers, the cleaning actions become evenly distributed throughout the year as this minimizes the total fouling. This is on a par with hypotheses postulated by Trafczynski et al. [42] that the ideal HEX cleaning schedule would have cleaning actions with an even distribution. For instance, in the case with three actions, the number of periods between cleaning actions (first and last periods included) is 9, 10, 9, and 9, respectively. Since the cleaning actions’ possible occurrence times are integer, some periods between cleaning are longer.

For four cleaning actions, it is possible to notice two actions occur in the same period. As the objective function counts unique values of CIPs for each heat exchanger, this effectively means only three actions occur. As they represent the best result, data for three cleaning actions are displayed to better understand the behavior of the system.

The best result is reached within five iterations. As the PSO has a high number of particles, a good solution is already found in its first iteration. By iteration eleven, all particles have already stagnated into the best result found. Although there is no guarantee of convergence into a minimum, the results found are good, and as the number of cleaning actions are changed, the results are consistent with each other.

When cleaning actions occur, there is a sudden drop in resistance followed by another period of zero resistance. This happens because, while the HEX is being cleaned, it is not in operation, so no fouling occurs. Although the tube-side coke resistance is low, it makes a difference in the total fouling width and the system’s hydraulics overall. The slow aging rate occurs because the aging ODE rates depend on gel fouling width, which is negligible in the periods after cleaning actions take place. For this case study, the CIPs were set up in a way to keep the maximum fouling resistance as constant as possible, at around $0.003 \text{ m}^2 \cdot \text{K} \cdot \text{W}^{-1}$. The maximum width was about 0.40 mm or 4.2% of the clean inner radius. Figure 1 shows the HEX (a) and furnace (b) load for this case study.

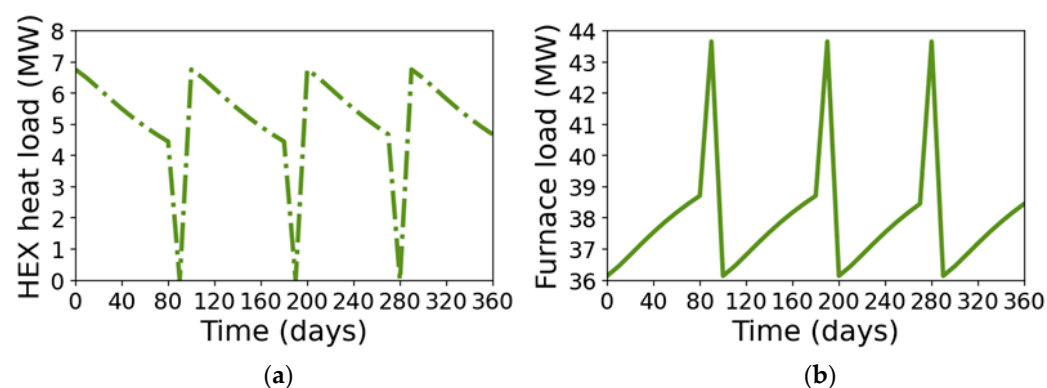


Figure 1. HEX (a) and furnace (b) loads over time for Case Study 1.

As displayed in Figure 1, the HEX load drops over time as resistance increases. This shows that even low resistance values have a high impact on HEX efficiencies. Naturally, as the HEX load decreases, the furnace load must be increased to offset losses. It is also noticeable that stopping a heat exchanger for a cleaning action has greatly increased furnace loads during the associated period.

The pressure drop starts at about 100 kPa and increases over time as the inner radius decreases. Pump power has the same behavior. However, when it is compared to the HEX heat load, pump power has a much lower order of magnitude (20 to 25 kW), which is added to the total costs, as pressure drops are already calculated and only one additional calculation is required for all periods.

3.2. Case Study 2

Case Study 2 is constituted of two HEXs (with one shell each) in parallel. Each of the heat exchangers is equal to the one in Case Study 1. The fluids considered are also crude oil (tube) and vacuum residue (shell), with the same inlet temperatures and mass flow rates. Figure 2 shows a representation of the studied system.

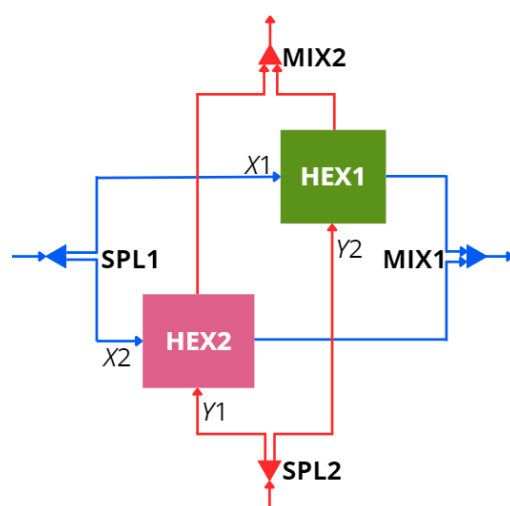


Figure 2. Heat exchanger network for Case Study 2.

As seen in Figure 2, Case Study 2 is composed of two heat exchangers, two splitters, and two mixers. The number of cleaning actions was also varied for Case Study 2. Table 5 displays the main results related to the HEN as cleaning actions are added to the process.

Table 5. Computation times (CT), HEN duty, furnace energy, carbon footprint, total costs, and cleaning periods (CIPs) for Case Study 2.

Parameter	Unit	3 Actions	4 Actions	5 Actions	6 Actions
Total CT	s	13.46	12.65	12.63	11.97
ODE CT	s	4.90	4.90	4.86	4.64
P-driven CT	s	6.50	6.50	6.57	6.22
HEN duty	MWh	47,479.6	49,751.6	51,201.6	52,576.5
Furnace energy	MWh	335,262.7	332,738.4	331,127.2	329,599.5
Carbon emitted	ton	3687.9	3660.1	3642.4	3625.6
Total costs	USD	9,252,732	9,213,739	9,199,706	9,187,956
HEX1 CIPs	-	{11,25}	{10,23}	{8,18,28}	{8,17,27}
HEX2 CIPs	-	{18}	{12,25}	{12,24}	{9,19,28}

As seen in Table 5, the average time taken for optimization was 12.67 s, of which an average of 4.83 s was taken estimating ODE values and 6.45 s was used to estimate pressure-driven mass flow. When compared to Case Study 1, the total time cost was increased by 7.8 s or 161%. However, most of this time increase may be attributed to pressure-driven estimations. Comparing the ODE time costs directly, there was an increase of 1.14 s or 31% for an additional HEX; in other words, the number of equations doubled, but only 31% more time was needed. This is evidence that solving all HEX calculations at once using NumPy, as described in the Supplementary Material, increases the coding efficiency. When compared to the literature [34], the code presents fast stagnation. Lozano-Santamaria and Macchietto [34] took 319.96 s to determine the number of cleaning actions and their allocation. Since there are four possible allocations, as the number of cleaning actions in that work was capped at two per HEX, the equivalent time for this work would be only 50.72 s. However, the comparison here may be unfair, as that work presented simultaneous cleaning allocation optimization and shell-side mass flow rate control.

For Case Study 2, six cleaning actions yielded the best results with a cost of USD 9,187,956 for a year. However, as four cleaning actions cost USD 9,213,739, or USD 25,783 more, this was considered a better result, as operationally adding two cleaning actions for such small savings would not be reasonable. Added to that, the difference in cost is not enough to justify the added risk of more cleaning actions, as cleaning costs could run higher than the predicted USD 30,000, due to unpredictable events. Taking four cleaning actions represents a reduction of USD 38,993 compared to the three cleaning actions option.

In this case, study, where there is an interaction between HEXs, the Trafczynski et al.'s [42] hypothesis of evenly distributed cleaning actions does not hold completely. However, in the four-action case, HEX2 has intervals of 12, 13, and 12, while HEX1 has intervals of 10, 13, and 14. The space between cleaning actions was 13 periods for both HEXs. This shows that HEX2 was prioritized by being evenly distributed, while HEX1's first period was shifted to period 10.

Furthermore, as both heat exchangers have the same design, for three cleaning actions, cleaning HEX1 two times and HEX2 one time or HEX2 two times and HEX1 one time would yield the same cost result each other. Similarly to Case Study 1, when one more cleaning action was added, totaling seven (not provided in Table 5), the best solution turned two cleaning actions into one by putting them into the same period.

PSO takes about eight iterations to find the lowest value and about thirteen iterations to stagnate.

The rate of fouling is much higher, compared to Case Study 1, as the crude oil stream is divided into two. Therefore, Equation (2) receives much lower Reynolds numbers and shear stress values as input, increasing the fouling rate. The maximum fouling resistance reached by HEX1 and HEX2 were 0.0063 and 0.0057 $\text{m}^2 \cdot \text{K} \cdot \text{W}^{-1}$, respectively. These values

are about double the ones in Case Study 1. Figure 3 shows the tube (a) and shell (b) mass flow rate distribution through the studied periods.

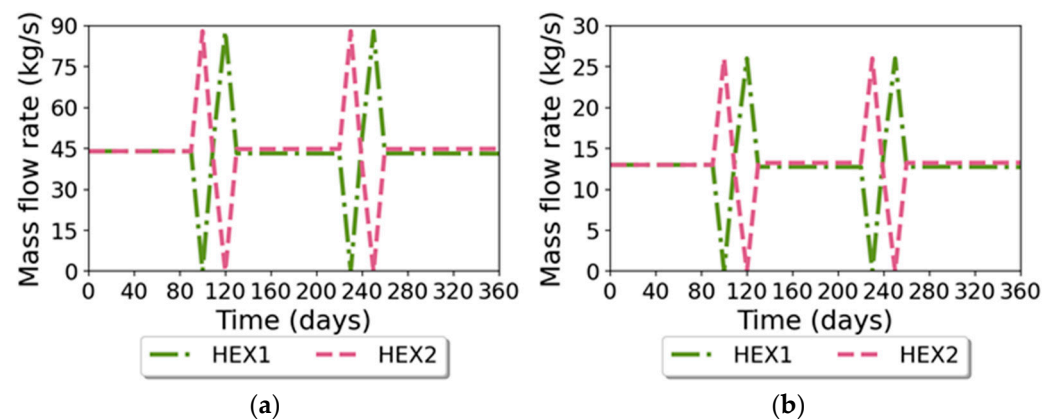


Figure 3. Mass flow rate distribution for the tube (a) and shell (b) sides of each heat exchanger for Case Study 2.

When all HEXs in a branch are being cleaned, the mass fraction of the functioning branch is set to one. Therefore, it receives all mass flow. Figure 3 shows that, after a heat exchanger is cleaned, it receives higher mass flow rates than the dirty HEX, so that the pressure-driven restriction may be respected. For instance, after HEX2 is cleaned in period 12, it receives about 0.51 of the total mass fraction. This behavior is repeated after every cleaning action. The shell side receives a mass flow rate proportional to the tube mass fraction. This simple operational approach led to USD 52,101 lower costs when compared to a set flow fraction of 0.5 on the shell side. Figure 4 shows how the HEX (a) and furnace (b) loads behave over time, for the proposed cleaning schedule.

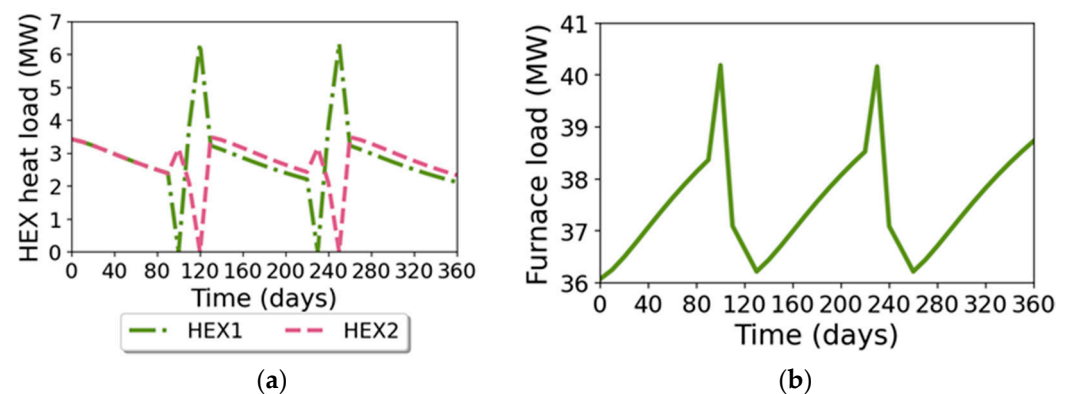


Figure 4. HEX (a) and furnace (b) loads over time for Case Study 2.

As seen in Figure 4, as a heat exchanger is being cleaned, there is a bump in the operating HEX's heat load. However, as the operating HEX has a reduced area and heat transfer coefficients, the increase in efficiency is modest when the exchanger has not been cleaned for a long period. This may be the reason both HEXs are cleaned so closely to each other.

Pressure drop values for Case Study 2 are generally much lower when compared to Case Study 1, as the HEXs receive only half of the mass flow rate. However, as this leads to higher fouling rates and lower flow areas, pressure drops during cleaning actions are much higher in the operating HEX, reaching upwards of 161 kPa. Pump power is much lower in this case study as well, but this has little impact on the objective function, as pump power is orders of magnitude lower than HEX loads.

3.3. Case Study 3

Case Study 3 consists of two HEXs in a countercurrent, as depicted in Figure 5. Both HEXs have the same design as the one presented in Case Study 1. The considered fluids are crude oil and vacuum residue, with the same inlet temperatures and mass flow rates, and cold fluid on the tube side. The intermediary temperatures of countercurrent nodes must be estimated, as they are needed to calculate the fouling rates in each shell. As mentioned in the hypotheses, when a heat exchanger is in series with others and is stopped for cleaning, the HEX is considered bypassed, while the others are considered to operate normally. This scenario occurs in Case Studies 3, 4, and 5.

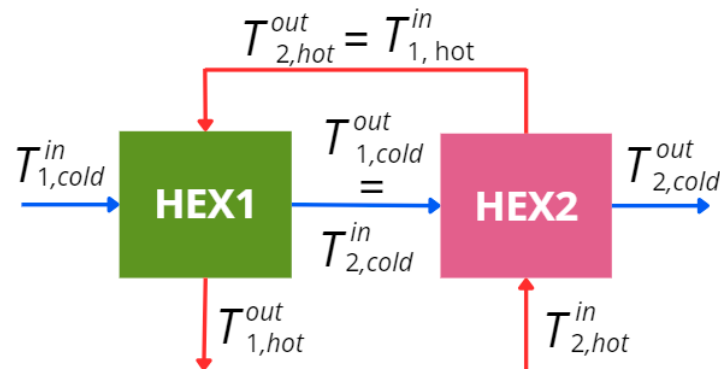


Figure 5. Heat exchanger network for Case Study 3.

The number of cleaning actions was also varied for Case Study 3. However, as the countercurrent loop also has an analytical solution, some cases were solved more than once to showcase the difference in computation times. Table 6 displays the main results related to the HEN in this case study.

Table 6. Computation times (CT), HEN duty, furnace energy, carbon footprint, total costs, and cleaning periods for Case Study 3.

Parameter	Unit	4 Actions	4 Actions *	5 Actions	5 Actions
Total CT	s	19.57	7.54	19.49	20.45
ODE CT	s	4.57	5.20	4.62	5.01
CC CT	s	13.90	0.87	13.81	14.57
HEN duty	MWh	59,902.8	59,902.8	60,874.6	61,015.92
Furnace energy	MWh	321,088.6	321,088.6	320,008.7	319,851.71
Carbon emitted	ton	3532.0	3532.0	3520.1	3518.37
Total costs	USD	8,895,350	8,895,350	8,895,838	8,891,547
HEX1 CIPs	-	{14,27}	{14,27}	{7,17,28}	{12,24}
HEX2 CIPs	-	{9,22}	{9,22}	{12,24}	{8,18,28}

* The analytical solution was used for this test.

As seen in Table 6, the average time taken for optimization was 19.83 s, of which an average of 4.73 s was taken estimating ODE values and 14.09 s was used to estimate countercurrent intermediary temperatures. When compared to Case Study 1, the total time cost was increased by 14.99 s or 309%. However, most of this time increase may be attributed to countercurrent temperature estimations. Comparing the ODE time costs directly, there was an increase of 1.05 s, or 29%, for an additional HEX. The analytical solution for two shells in a countercurrent proved much faster, as its countercurrent temperature estimation took only 0.87 s and the total time cost was 38% of its solver counterpart. As two shells in a countercurrent are a commonly used configuration, this simple substitution has the potential to greatly reduce the computation times of heat exchangers with fouling simulations.

Similarly, Case Study 2 code was run in an average of 12.68 s, while this case study needed an average of 19.84 s for the solver solution and 7.54 s for the analytical solution. Even though the pressure-driven estimation comes from a set of nonlinear equations and the P-NTU temperature estimations are linear, the pressure-driven equations still demonstrate better performance. This suggests there is still room for improvement in the presented temperature estimation solution. However, this solution is still fast when compared to other authors. For instance, the code from Lozano-Santamaria and Macchietto [34] needed 484 s to determine the number of cleaning actions and the optimal allocation. As there are only four possible allocations of a number of cleaning actions (as the authors have capped the system to two cleaning actions), this code's time equivalent would be 79.36 s, or 16.4% of their computation time, or 30.16 s when using the analytical solution (6.2% of their computation time).

In this case, there is also an interaction between HEXs, and that challenges Trafczynski et al.'s [42] hypothesis that evenly distributed cleaning actions are optimal. In the scenario with four cleaning actions, HEX1 has intervals of 14, 13, and 10, while HEX2 has intervals of 9, 13, and 15. The interval between cleaning actions was 13 periods for both HEXs. This indicates that due to the synergetic behavior of heat exchangers in a countercurrent, the most effective solution was symmetric. This outcome is partially attributed to both HEXs having the same design.

For Case Study 3, five cleaning actions yielded the best results with a cost of USD 8,895,838 when the colder HEX was cleaned three times or USD 8,891,547 when the hotter HEX was cleaned three times. However, similarly to Case Study 2, the difference between five and four cleanings was low (USD 488 and USD 3,803, respectively, which represent no more than 0.5% of the cost with four cleaning tasks). Therefore, as it is operationally sounder to have one less cleaning action, the case with four cleaning actions was considered better and their results are detailed in the following.

As HEX2's inlets have the highest temperatures in the system, the fouling rates are much higher than the ones in HEX1. Therefore, the PSO prioritizes cleaning HEX2 first, because of this difference in fouling rates. For reference, HEX1 reached a maximum resistance of $0.0037 \text{ m}^2 \cdot \text{K} \cdot \text{W}^{-1}$, while HEX2 reached $0.0050 \text{ m}^2 \cdot \text{K} \cdot \text{W}^{-1}$. Figure 6 shows the HEX (a) and furnace (b) loads over time.

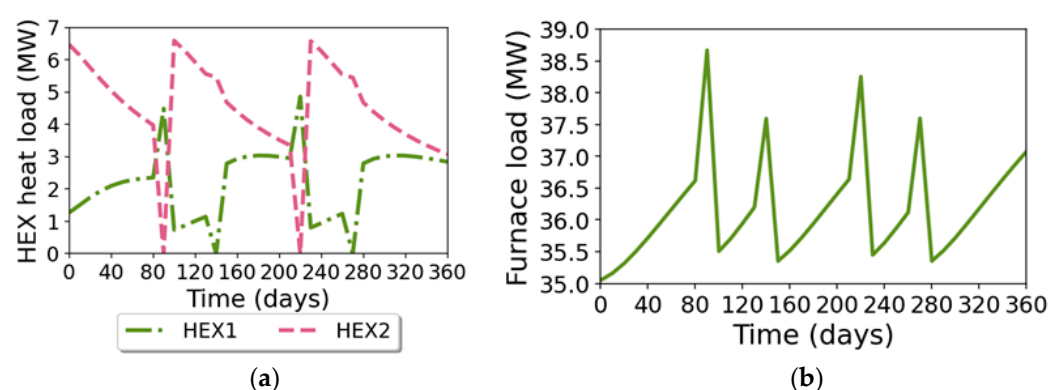


Figure 6. HEX (a) and furnace (b) loads over time for Case Study 3.

As seen in Figure 6, the furnace load behaves similarly to the previous case studies. However, HEX1's heat load behaves counterintuitively, since, as HEX2 loses efficiency and HEX1 has lower fouling rates, HEX1 heat load increases over time, stagnating at about 3 MW from period 15 to 21. This shows the efficiency of putting shells in a countercurrent for systems with fouling, as this creates a mechanism to counterbalance the hotter heat exchanger's efficiency loss.

At first glance, it may seem that fouling is not relevant in HEX1 when comparing only heat loads. However, when looking at estimated resistances or corrected efficiency charts [47], this is proven not to be the case as the higher temperature gradient counteracts the existing fouling. This case study significantly outperformed Case Study 2 when considering four cleaning actions, even though both case studies use the same heat exchangers. The HEN in Case Study 3 outperforms those of Case Studies 1 and 2 by USD 397,207 and USD 304,356, respectively. The superior performance can be attributed to the heat exchangers (HEXs) being designed for a tube flow rate of 88 kg/s. In Case Study 2, the flow rate was reduced to half the nominal value, which greatly increased fouling. This highlights the critical importance of proper HEX design. In relation to pressure drops, the countercurrent system behaves similarly to the one in Case Study 1. However, the increase in pressure drop occurs faster in HEX2, as it has higher fouling widths.

3.4. Case Study 4

Case Study 4 involves four heat exchangers (HEXs), each with a single shell, arranged in a parallel configuration. In this setup, each branch between the splitter and mixer contains two heat exchangers operating in a countercurrent flow arrangement. Figure 7 shows a representation of the studied system.

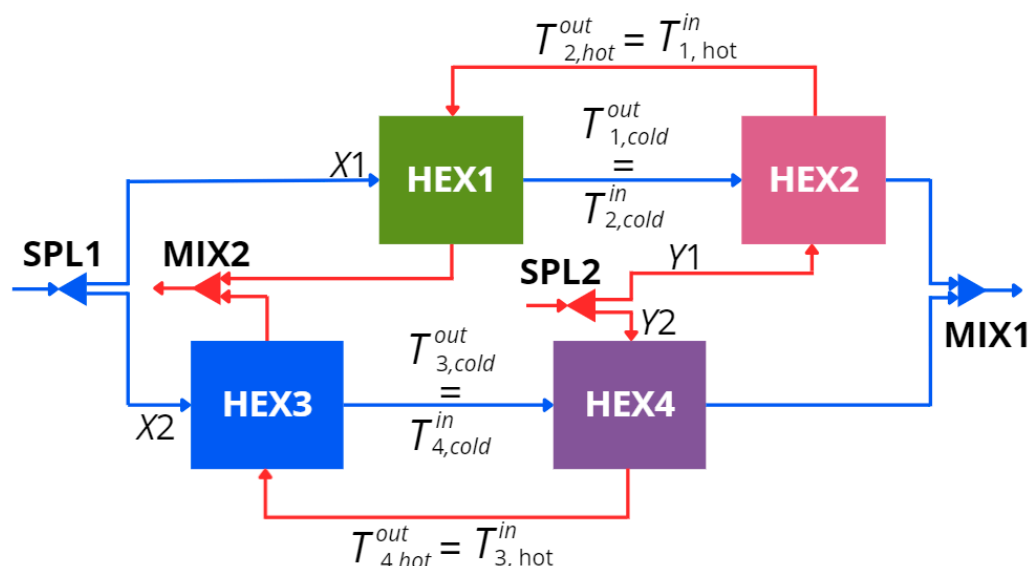


Figure 7. Heat exchanger network for Case Study 4.

As seen in Figure 7, Case Study 4 is composed of four heat exchangers, two splitters, and two mixers. The heat exchangers are equal and their parameters were adapted from Lozano-Santamaria and Macchietto [34] and represent part of a HEN introduced in that work. The considered fluids are crude oil (tube side) and vacuum residue (shell side), which have a total mass flow rate of 88 and 44 kg s⁻¹, respectively. The total mass flow rate is fed into the splitter and divided, which turns the mass flow rates of heat exchangers into variables. HEX and model parameters are displayed in Table 3. Table 7 displays the main results related to the HEN as cleaning actions are added to the process.

As seen in Table 7, the average time taken for the optimization was 19.73 s, of which an average of 7.38 s was taken estimating ODE values and 9.40 s was used to estimate pressure-driven mass flow rates. When compared to Case Study 1, the total time cost was increased by 14.88 s or 307%. However, most of this time increase may be attributed to pressure-driven estimations. Comparing the ODE time costs directly, there was an increase of 3.70 s or 100% for three additional HEXs. Since this case study only represents a part of

the HEN presented by Lozano-Santamaria and Macchietto [34], time comparisons are not made as they would have little meaning.

Table 7. Computation times, HEN duty, furnace energy, carbon footprint, total costs, and cleaning periods (CIPs) for Case Study 4.

Parameter	Unit	7 Actions	8 Actions	8 Actions	9 Actions
Total CT	s	20.64	19.57	19.23	19.48
ODE CT	s	7.63	7.38	7.12	7.39
P-driven CT	s	9.81	9.40	9.23	9.16
HEN duty	MWh	112,354.5	113,944.4	115,645.0	115,857.1
Furnace energy	MWh	262,808.9	261,042.3	259,152.7	258,917.0
Carbon emitted	ton	2890.9	2871.5	2850.7	2848.1
Total costs	USD	7,392,566	7,374,285	7,322,644	7,346,203
HEX1 CIPs	-	{29}	{17}	{11,24}	{16,28}
HEX2 CIPs	-	{10,23}	{8,17,25}	{9,22}	{9,20,30}
HEX3 CIPs	-	{11,25}	{12,26}	{13,26}	{10,21}
HEX4 CIPs	-	{11,25}	{12,26}	{13,26}	{10,21}

For Case Study 4, eight cleaning actions yielded the best results with a cost of USD 7,322,644 for a year. Shell mass fractions were set to be equal to tube mass fractions. For the sake of comparison, tests were run in which shell mass fractions were kept constant at 0.5, and these tests had worse results for all cleaning quantities. For instance, the total yearly cost for eight cleaning actions was USD 7,384,777, which suggests that the approach we used is operationally better.

Similar to previous case studies, the hypothesis proposed by Trafczynski et al. (2023) [42] is challenged. The intervals for this case study are {11,13,13}, {9,13,15}, {13,13,11}, and {13,13,11} for HEXs 1, 2, 3, and 4, respectively. HEX2 and HEX1 are offset from being evenly distributed by four and two periods, respectively. This is due to an order of priority found by the PSO, in which the hotter end is generally set to be cleaned before the colder end for each branch. In this particular case study, one branch was set up to receive all mass flow during periods 13 and 26.

Maximum fouling resistance varied between HEX1/HEX3 (colder end) and HEX2/HEX4, which were 0.0069 and $0.0090 \text{ m}^2 \cdot \text{K} \cdot \text{W}^{-1}$, respectively. This is due to the high influence of temperature on fouling rates. Figure 8 shows the HEX (a) and furnace (b) loads over time, for the case with two cleaning actions for each HEX.

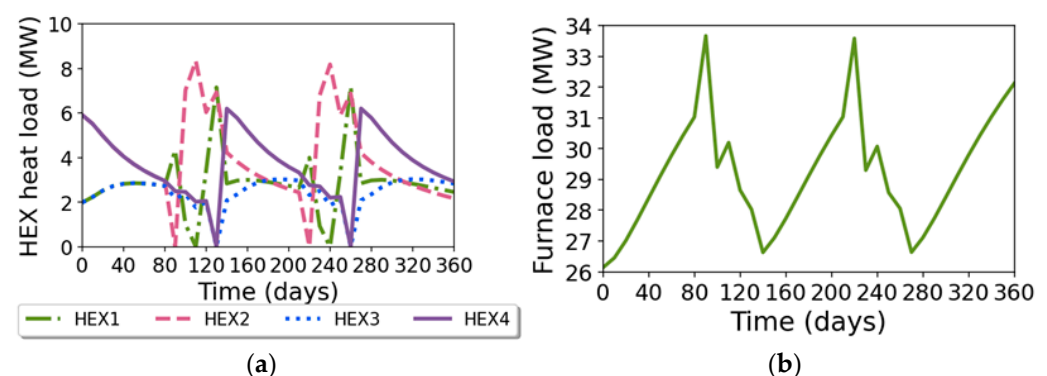


Figure 8. HEX (a) and furnace (b) loads over time for Case Study 4.

As seen in Figure 8, as an entire branch is being cleaned (periods 13 and 26), it is possible to notice a bump in the operating branch's heat load. However, when only one heat exchanger of a branch is cleaned, more flow is redirected to the branch with one operating HEX. For instance, on days 90 and 110, there is a drop in HEX3 and HEX4's hex

loads precisely because they receive a smaller flow than HEX1 (day 90) and HEX2 (day 110). Figure 9 shows the tube (a) and shell (b) mass flow rate distribution through the studied periods, where Branch 1 represents HEX1 and HEX2, and Branch 2 represents HEX3 and HEX4.

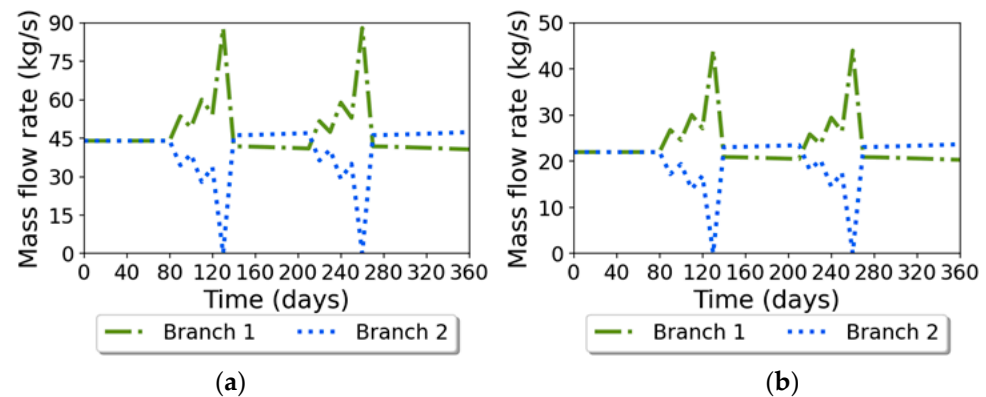


Figure 9. Tube (a) and shell (b) mass flow rates by branch for Case Study 4.

Figure 9 demonstrates that, after a heat exchanger is cleaned, its branch receives a higher mass flow rate than the dirty branch to comply with the pressure-driven restriction. This highlights the optimal strategy of cleaning the branch that will receive the full mass flow before the flow is redirected to it. This pattern is particularly evident in periods 9, 11, and 13. In these periods, the flow rate in Branch 1 increases from periods 9 to 11 as the heat exchangers in this branch are cleaned. Then, in period 13, when Branch 2 undergoes maintenance, the entire flow is directed to Branch 1.

This approach is effective because the heat exchangers in Branch 1 (HEX1 and HEX2) are cleaned just before this shift, preparing the branch to maximize its heat load. This strategy is chosen because, when only one heat exchanger is stopped, most flow goes to the branch with a single functioning heat exchanger, due to the lower pressure drop compared to an entire branch. This is seen in periods 9 and 11, when HEX2 and HEX1 are being cleaned, and most flow goes to Branch 1, which has only one heat exchanger in operation.

When looking at pressure drops and pumping power, it becomes evident that completely stopping a branch may not be operationally feasible, as the required pumping power increases from 7.5 to 33.3 kW in HEX1 and 8.7 to 39.9 kW in HEX2. It also may present damage to the equipment over time, as pressure drops reach as high as 200 kPa. Therefore, pressure drop upper limit restrictions could be implemented in future work to ensure operability, which would mean bypassing some of the fluid when an entire branch is stopped for cleaning or avoiding this situation.

3.5. Case Study 5

Case Study 5 refers to the cleaning optimization of four heat exchangers in a series and countercurrent, adapted from Lozano-Santamaria and Macchietto [34]. The used tube-side fluid was crude oil and the shell-side fluid was light gas oil (LGO), which have mass flow rates of 88 and 70 kg s⁻¹ and inlet temperatures of 403.15 and 530.15 K, respectively. This HEN is part of a larger HEN introduced in that work. Therefore, the proposed HEN does not feed directly into the furnace. Consequently, COT and furnace loads are replaced by more appropriate terms, such as target temperature (493 K) and additional furnace load, as the changes in this HEN's outlet temperature would still influence the furnace load. The shell-side fouling rate was set to zero for this case study, as light gas oil is a lighter fraction of crude oil. As seen in Table 3, HEX1 and HEX2 are different than HEX3 and HEX4. The first two HEXs are smaller than the last two. As temperatures are low, the first two HEXs

have the suppression coefficient of the Ebert–Panchal equation set to zero. Figure 10 shows a diagram representing the heat exchanger network of Case Study 5.

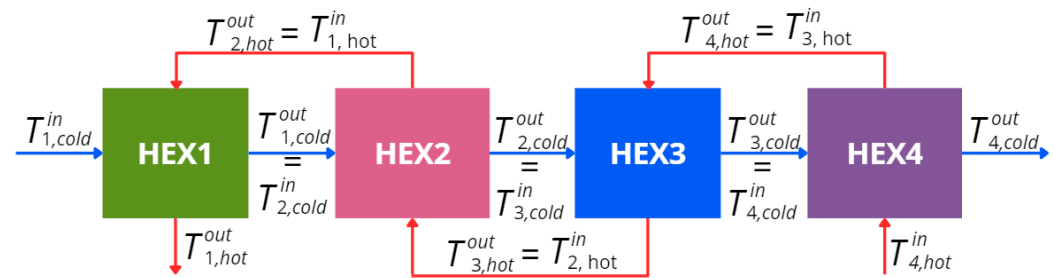


Figure 10. Heat exchanger network for Case Study 5.

The first step taken was to vary the number of cleaning actions set for the heat exchangers. Table 8 displays the main results related to the HEN as cleaning actions are added to the process. The results are related to the partial analytical solution, in which the analytical solution is applied to each pair, HEX1/HEX2 and HEX3/HEX4. Therefore, the only countercurrent unknown variable is reduced to the shell-side outlet temperature of HEX3.

Table 8. Computation times (CT), HEN duty, furnace energy, carbon footprint, total costs, and cleaning periods (CIPs) for Case Study 5.

Parameter	Unit	8 Actions	8 Actions	9 Actions	10 Actions
Total CT	s	47.02	46.29	51.76	52.66
ODE CT	s	6.26	6.17	7.03	6.86
cc CT	s	39.70	39.18	43.55	44.75
HEN duty	MWh	174,062.8	174,642.6	175,618.8	176,631.0
Energy to 493 K	MWh	28,656.8	28,012.6	26,927.9	25,803.3
Carbon emitted	ton	315.2	308.1	296.2	283.8
Total costs	USD	1,023,191	1,005,585	1,005,939	1,005,203
HEX1 CIPs	-	{16,29}	{17}	{15,27}	{13,23}
HEX2 CIPs	-	{11,24}	{13,26}	{13,25}	{12,25}
HEX3 CIPs	-	{13,26}	{10,23}	{9,22}	{8,18,28}
HEX4 CIPs	-	{9,22}	{8,19,29}	{8,19,29}	{7,17,27}

As seen in Table 8, the average time taken for optimization was 49.43 s, of which an average of 6.58 s was taken estimating ODE values. For comparison purposes, a non-analytical solution was carried out, taking a total time of 228.8 s. This shows that the partial analytical solution greatly simplifies the problem, making the optimization much faster. Since this case study also only represents a part of the HEN presented by Lozano-Santamaria and Macchietto [34], time comparisons are not made as they would have little meaning.

For Case Study 5, eight cleaning actions yielded the best results with a cost of USD 1,005,585 for a year. The first eight cleaning actions column, in which HEX1 and HEX4 are cleaned two times, was USD 17,606 more expensive than the second one, in which HEX1 and HEX4 are cleaned one and three times, respectively. The best result also displayed functionally equal monetary values to the nine and ten cleaning actions cases. However, 11.9 and 24.3 tons of carbon emissions are saved with additional cleanings, when compared to the considered best case. This represents a 3.9 and 7.9% decrease in emissions. On the other hand, the emissions of cleaning products used are not considered in the estimation and this may counterbalance this difference.

Similar to previous case studies, the hypothesis proposed by Trafczynski et al. [42] is challenged. The intervals for this case study are {17,20}, {13,13,11}, {10,13,14}, and {8,11,10,8}

for HEXs 1, 2, 3, and 4, respectively. This is due to an order of priority found by the PSO, in which the hotter end is generally set to be cleaned before the colder end.

All heat exchangers were found to have about the same maximum fouling resistance, between 0.0016 and $0.0025 \text{ m}^2 \cdot \text{K} \cdot \text{W}^{-1}$. Shell-side fouling resistances were set to zero and tube-side coke resistances were lower than in other case studies as temperatures were much lower (ranging from 403 to 490 K on the tube side). Although three cleaning actions were assigned to HEX4, it has the highest fouling values, as it is on the hot end of the HEN. Figure 11 shows the HEX (a) and furnace (b) loads over time.

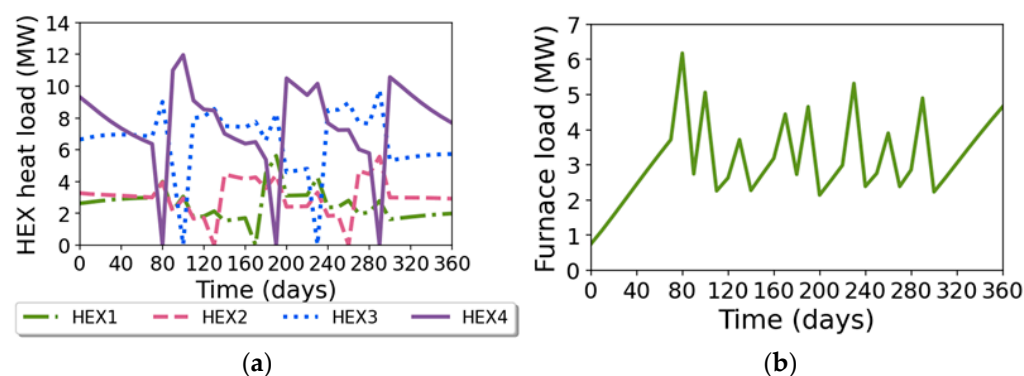


Figure 11. HEX (a) and additional furnace (b) loads over time for Case Study 5.

As seen in Figure 11, the furnace load behaves similarly to other case studies. HEX loads also behaved similarly and, as HEX4 got dirtier at the beginning of the studied period, the other HEXs increased their heat loads. During cleaning periods, one HEX being out of operation makes the additional furnace load peak and, in the next period, the load decreases as there is a new clean HEX in the countercurrent system.

As HEX1/HEX2 and HEX3/HEX4 have different parameters, the initial pressure drops and pump power are different. For both designs, the pressure drop increase occurs faster in hotter HEXs (HEX2 and HEX4). Even though pressure drops are higher in HEX3/HEX4, Reynolds number values start roughly the same for all HEXs, as HEX1/HEX2 have roughly half the number of tubes.

3.6. Overall Trends

As discussed in Section 2.2, the model considered ten-day periods. To evaluate the sensitivity of the objective function to this period length, a five-day period was tested in Case Study 4. The results showed a slight shift in the decision variables, with cleaning actions for HEX1, HEX2, HEX3, and HEX4 scheduled to begin on days {110,240}, {95,225}, {135,265}, and {135,265}, respectively. This represents a five-day difference for HEX2, HEX3, and HEX4 compared to the ten-day period scenario. The objective function value decreased by just under USD 1000 when comparing the previous and new solutions (both considering the five-day period scenario), but this improvement came at the cost of increased computation time, which rose from 19.7 to 34.2 s. Given the minimal gain and the potential introduction of additional optimization variables, implementing the five-day period was not deemed worthwhile.

Comparing the solution presented in Case Study 4 (ten-day periods) to the five-day period scenario, costs increased by USD 40,000 due to more frequent updates of fouling resistances. In the ten-day scenario, resistances are updated on the tenth day, while in the five-day scenario, they are updated on the fifth day. This higher frequency of updates leads to increased costs, representing a 0.5% rise in total expenses. Therefore, when more precise results are required, using smaller periods should be considered. Additionally, period lengths longer than ten days were not considered because the current implementation does

not support resetting fouling values within the ODE solver. As a result, increasing the period length would require calculating the ODE values for each particle separately, leading to higher computation times. Since the time cost per particle decreases as the number of particles increases, maintaining ten-day periods helps preserve computational efficiency. Therefore, longer periods options were not pursued.

Fouling rates in this study are higher compared to those reported in the literature [34]. This discrepancy arises due to different methods of aging estimation. Specifically, this study considers slower aging rates, leading to higher fouling rates due to smaller tube Reynolds numbers. Additionally, those authors [34] did not consider shell-side fouling. These methodological differences led the optimization solver to set a higher number of cleaning actions for any given heat exchanger. The timing and frequency of these cleaning actions are crucial for optimizing the HEN's performance, impacting both operating costs and the carbon footprint. Therefore, the economic values differ significantly between the two studies, even though the HENs in this work are based on their design. Notably, an increase in the number of cleaning actions across all case studies was observed, aligning with expectations. For instance, the cleaning schedule in Case Study 2 results in total savings of USD 372,000 compared to a scenario with no cleaning actions. In contrast, Lozano-Santamaria and Macchietto [34] reported USD 223,000 in savings. The difference in savings is primarily due to the higher fouling rates observed in this study, which stem from slower aging rates, as well as the omission of shell-side fouling in their study. These differences led the optimization solver to recommend more frequent cleaning actions for each heat exchanger in this study. As a result, the observed savings are higher, which is consistent with the expectations given the increased number of cleaning actions across all case studies.

The differences observed between this study and the previously reported work [34] highlight the significance of fouling parameters, including fouling and aging rates. A sensitivity analysis of the influence of these parameters on individual heat exchangers has been conducted in previous studies [11,12]. However, further investigation into their effects on the cleaning schedules of individual HEXs and complete HENs would be valuable.

Managing pressure-driven flow is critical for maintaining HEN efficiency and preventing operational issues such as excessive pressure drops. Simple operational maneuvers, such as setting, among the heat exchangers in parallel, equal mass fractions for the tube (SPL1) and shell (SPL2) sides, have proven to be effective in reducing costs. In other words, maintaining the same proportion of flow in each branch for both SPL1 and SPL2 has reduced the objective function value. Additionally, implementing allowable pressure drop limits might be necessary if the system under study has a low pumping surplus.

There is a nonlinear relationship between the number of cleaning actions and the overall cost and performance of the HEN. As the number of cleaning actions increases, their benefits diminish. Optimal cleaning schedules are often asymmetric, favoring certain heat exchangers over others based on their fouling rates, designs, and positions within the network. This finding challenges the hypothesis that cleaning actions should be distributed at regular intervals [42]. However, the case studies presented in this work have a one-year timeframe, and this asymmetric behavior could change for longer timeframes.

The observed asymmetry prevents the system from having too many HEXs with high fouling resistances at once. This trend was more accentuated for HEXs in a countercurrent, as one HEX is better able to compensate for the high resistances of another. Additionally, HEXs with higher temperatures require to be cleaned more frequently and before those with lower temperatures, as fouling rates are temperature-dependent.

While the full implications for HEN design are difficult to fully capture without conducting optimization, this asymmetry suggests that there could be advantages to using

two single-shell heat exchangers (which could be stopped individually) in a countercurrent arrangement, rather than a single two-shell heat exchanger. This design approach would help avoid the issue of needing to stop both heat exchangers simultaneously. This concept should be explored in more detail in future research.

A notable pattern emerged, in which HEXs set to be cleaned twice always had 13 periods between cleaning actions, and those set to be cleaned three times had an interval of about 10 periods. In the work by Trafczynski et al. [42], the authors proposed that cleaning actions should be isospaced, meaning that cleaning actions should be evenly distributed throughout the studied period, and they optimized the number of cleaning actions for each HEX. In contrast, our approach involved setting the number of cleaning actions and optimizing their distribution. We observed that cleaning actions should indeed be isospaced, but we also found that the first cleaning period should be shifted to avoid cleaning too many heat exchangers simultaneously.

Lastly, it is important to note that the code used in this study was a proof of concept, with the number of PSO iterations left unnecessarily high. Therefore, the results presented here could be achieved with even lower computation times.

4. Conclusions

An integer particle swarm optimization (PSO) method for optimizing the cleaning schedules of several heat exchanger networks (HENs) under fouling (on both sides) and aging (on the tube side) was developed. Five HENs with varying complexity were studied. Computation times were kept low by focusing on improving high-demand parts of the code, such as countercurrent temperature estimation, pressure-driven flow distribution, and fouling rate estimation. While PSO was a suitable choice for this study, we plan to explore and test other population-based methods in future research. A greater number of cleaning actions were necessary to sustain HEN performance due to the addition of shell-side fouling rates and the usage of lower aging rates, resulting in notable economic discrepancies with other studies. Additionally, the effective management of pressure-driven flow was identified as crucial for enhancing HEN efficiency and reducing costs, with simple operational adjustments proving impactful. The observed interval patterns offer insights into potential improvements in cleaning strategies.

When comparing Case Studies 1, 2, and 3 (which share the same fluid types and parameters), the countercurrent HEN (CS3) outperforms the other two. The countercurrent configuration counteracts the effects of fouling, because, as the temperature difference between the cold and hot inlet increases in HEX1 (due to fouling in HEX2), HEX1's heat load increases, despite fouling. This leads to the Case Study 3 HEN outperforming the others by more than USD 300,000.

Overall, this research contributes valuable insights into HEN optimization and highlights the importance of addressing methodological nuances in future studies. In future research, it is recommended to incorporate shell-side threshold models and consider Bell–Delaware parameters as variables. This study revealed that temperature estimation in countercurrent loops posed a significant bottleneck, suggesting the necessity of adopting a more suitable method. Additionally, the importance of a well-designed heat exchanger (HEX) for achieving favorable results was demonstrated. Therefore, future endeavors could leverage the low computation costs achieved in this study by integrating the optimization of cleaning schedules with HEN design optimization.

While direct validation with plant data was not within the scope of this work, the robustness and accuracy of the underlying fouling models lend credibility to the results. Future work could include additional validation with specific plant data to further align the

findings with industrial applications as the results of this research have significant applied value for refinery operators and industrial practitioners.

By optimizing cleaning schedules in HENs with more comprehensive modeling of fouling and aging phenomena, this study offers a practical solution for minimizing operating costs and improving energy efficiency. The reduction in fouling-related emissions also contributes to environmental sustainability, aligning with global efforts to lower industrial carbon footprints. Moreover, the proposed method offers a more computationally efficient solution, enabling the future incorporation of additional optimization variables, thereby enhancing their practical utility in real-world industrial applications.

Supplementary Materials: The following supporting information can be downloaded at: <https://www.mdpi.com/article/10.3390/en18010071/s1>. A detailed explanation of the programming logic is available in Supplementary Material File S1. Additionally, a file containing the most relevant variable values for each case study can be found in Supplementary Material File S2. Reference [48] is cited in the supplementary materials.

Author Contributions: Conceptualization, J.P.V.d.C., M.A.S.S.R., F.D.M., and C.B.B.C.; Methods, J.P.V.d.C., M.A.S.S.R., F.D.M., and C.B.B.C.; Computer code, J.P.V.d.C.; Investigation, J.P.V.d.C.; Resources, M.A.S.S.R., F.D.M., and C.B.B.C.; Data curation, J.P.V.d.C.; Writing—original draft, J.P.V.d.C.; Writing—review and editing, J.P.V.d.C., M.A.S.S.R., F.D.M., and C.B.B.C.; Visualization, J.P.V.d.C. and C.B.B.C.; Supervision, F.D.M. and C.B.B.C.; Project administration, C.B.B.C.; Funding acquisition, M.A.S.S.R., F.D.M., and C.B.B.C. All authors have read and agreed to the published version of the manuscript.

Funding: This research was funded by the National Council for Scientific and Technological Development—CNPq (Brazil), processes 307958/2021-3, 309026/2022-9, and 406544/2023-9, and the Coordenação de Aperfeiçoamento de Pessoal de Nível Superior—Brasil (CAPES), process 88887.714299/2022-00 and Finance Code 001.

Data Availability Statement: A detailed explanation of the programming logic is available in Supplementary Material File S1. Additionally, a file containing the most relevant variable values for each case study can be found in Supplementary Material File S2. For further information, the authors can be contacted directly.

Acknowledgments: The authors gratefully acknowledge financial support from the National Council for Scientific and Technological Development—CNPq (Brazil), processes 307958/2021-3, 309026/2022-9, and 406544/2023-9, the Coordenação de Aperfeiçoamento de Pessoal de Nível Superior—Brasil (CAPES), process 88887.714299/2022-00 and Finance Code 001, and the National Council on Scientific and Technical Research—CONICET (Argentina).

Conflicts of Interest: All authors declare that they have no conflicts of interest.

Nomenclature

Symbol	Meaning	Unit
A_a	Pre-exponential aging factor	day ^{−1}
B_c	Baffle cut	-
$C_{cleaning}$	Costs associated with cleaning each HEX in each period	USD
C_{CO_2}	Costs associated with carbon emission in each period	USD
C_{fuel}	Costs associated with fuel usage in each period	USD
C_p	Specific heat of a fluid	J·kg ^{−1} ·K ^{−1}
$C_{pumping}$	Additional cost of pumping for each HEX in each period	USD
$d_i^{clean} = 2r_i^{clean}$	Tube inner diameter or radius	mm
$D_i(t) = 2r_i(t)$	Current tube diameter or radius	mm

$d_o = 2r_o$	Tube outer diameter or radius	mm
$D_s = 2r_s$	Shell diameter or radius	m
E_a	Aging activation energy	$\text{kJ}\cdot\text{mol}^{-1}$
E_f	Fouling activation energy	$\text{kJ}\cdot\text{mol}^{-1}$
ff	Friction factor	-
G	Mass flux	$\text{kg}\cdot\text{m}^{-2}\cdot\text{s}^{-1}$
h_s	Shell-side heat transfer coefficient	$\text{W}\cdot\text{m}^{-2}\cdot\text{K}^{-1}$
h_s^i	Shell-side heat transfer coefficient for ideal crossflow	$\text{W}\cdot\text{m}^{-2}\cdot\text{K}^{-1}$
h_t	Tube-side convective coefficient	$\text{W}\cdot\text{m}^{-2}\cdot\text{K}^{-1}$
J_b	Correction factor for bundle bypass effects	-
J_c	Correction factor for segmental baffle window	-
J_l	Correction factor for leakage effects	-
J_r	Correction factor for laminar flow	-
J_s	Correction factor for unequal baffling spacing	-
k	Conductivity of a fluid	$\text{W}\cdot\text{m}^{-1}\cdot\text{K}^{-1}$
k_w	Wall conductivity	$\text{W}\cdot\text{m}^{-1}\cdot\text{K}^{-1}$
L_{bc}	Baffle spacing	m
L_t	Effective tube length	m
\dot{m}	Mass flow rate	$\text{kg}\cdot\text{s}^{-1}$
N_{HEX}	Number of heat exchangers	-
N_{per}	Number of periods	-
N_{pop}	Number of particles in the PSO	-
N_p^{shell}	Number of shell passes	-
N_p^{tube}	Number of tube passes	-
n_{seconds}	Number of seconds in the ten-day period	-
N_t	Number of tubes	-
NTU	Number of transfer units	-
OF	Objective Function	USD
Pr	Prandtl Number	-
Q	Heat load	W
Q_{furn}	Furnace load	W
Q_{pump}	Pumping power	W
rug	Tube rugosity	-
R	Universal gas constant	$\text{J}\cdot\text{mol}^{-1}\cdot\text{K}^{-1}$
Re	Reynolds number	-
R_f	Total fouling resistance	$\text{m}^2\cdot\text{K}\cdot\text{W}^{-1}$
$R_{f,c}$	Coke resistance	$\text{m}^2\cdot\text{K}\cdot\text{W}^{-1}$
$R_{f,g}$	Gel resistance	$\text{m}^2\cdot\text{K}\cdot\text{W}^{-1}$
S_1	Repeating friction factor equation parameter one	-
S_2	Repeating friction factor equation parameter two	-
S_3	Repeating friction factor equation parameter three	-
t	time	days
T_{avg}	Average temperature	K
T_f	Film temperature	K
T_{fg}	Fluid–gel interface temperature	K
T_{gc}	Gel–coke interface temperature	K
T_s^{in}	Shell inlet temperature	K
T_s^{out}	Shell outlet temperature	K
T_t^{in}	Tube inlet temperature	K
T_t^{out}	Tube outlet temperature	K
rug	Tube relative roughness coefficient	m
U	Overall heat transfer coefficient	$\text{W}\cdot\text{m}^{-2}\cdot\text{K}^{-1}$
α_1	Tube-side deposition coefficient	$\text{K}\cdot\text{m}^2\cdot\text{W}^{-1}\text{ day}^{-1}$
α_2	Shell-side deposition coefficient	$\text{K}\cdot\text{m}^2\cdot\text{W}^{-1}\text{ day}^{-1}$

γ	Suppression coefficient	$\text{m}^4 \cdot \text{K} \cdot \text{N}^{-1} \cdot \text{W}^{-1} \text{ day}^{-1}$
δ_c	Coke fouling width	mm
δ_g	Gel fouling width	mm
ΔP	Pressure drop	Pa
δ_{tube}	Total tube fouling width	mm
ϵ	Tube absolute roughness coefficient	mm
η_{furn}	Furnace efficiency	-
η_{pump}	Pump efficiency	-
λ_c	Coke thermal conductivity coefficient	$\text{W} \cdot \text{m}^{-1} \cdot \text{K}^{-1}$
λ_g	Gel thermal conductivity coefficient	$\text{W} \cdot \text{m}^{-1} \cdot \text{K}^{-1}$
μ	Fluid viscosity	$\text{Pa} \cdot \text{s}$
ρ	Density	$\text{kg} \cdot \text{m}^{-3}$
τ_w	Shear stress	Pa
Acronym	Meaning	Unit
CIT	Coil inlet temperature	K
CIPs	Cleaning periods	-
COT	Coil outlet temperature	K
CS	Case Study	-
CT	Computation time	s
HEN	Heat exchanger network	-
HEX	Heat exchanger	-
INLP	Integer nonlinear programming	-
MINLP	Mixed integer nonlinear programming	-
NLP	Nonlinear programming	-
PHT	Pre-heat train	-
P-NTU	Effectiveness-number of transfer units	-
PSO	Particle swarm optimization	-
VR	Vacuum residue	-
Subscript	Meaning	
f	Fouling	
f,c	Coke	
f,g	Gel	
s	Shell-side	
t	Tube-side	

References

1. Ishiyama, E.M.; Pugh, S.J.; Zettler, H.U. Economic and Environmental Implications of Fouling in Crude Preheat Trains. *Heat Transf. Eng.* **2023**, *45*, 1277–1285. [\[CrossRef\]](#)
2. Ishiyama, E.M.; Pugh, S.J.; Wilson, D.I. Incorporating Deposit Ageing into Visualisation of Crude Oil Preheat Train Fouling. *Process Integr. Optim. Sustain.* **2020**, *4*, 187–200. [\[CrossRef\]](#)
3. Diaz-Bejarano, E.; Coletti, F.; Macchietto, S. A new dynamic model of crude oil fouling deposits and its application to the simulation of fouling-cleaning cycles. *AIChE J.* **2016**, *62*, 90–107. [\[CrossRef\]](#)
4. Ishiyama, E.M.; Falkeman, E.; Wilson, D.I.; Pugh, S.J. Quantifying Implications of Deposit Aging from Crude Refinery Preheat Train Data. *Heat Transf. Eng.* **2020**, *41*, 115–126. [\[CrossRef\]](#)
5. Coletti, F.; Macchietto, S. Refinery pre-heat train network simulation undergoing fouling: Assessment of energy efficiency and carbon emissions. *Heat Transf. Eng.* **2011**, *32*, 228–236. [\[CrossRef\]](#)
6. Abdulhussein, Z.A.; Al-Sharify, Z.T.; Alzurairi, M.; Onyeaka, H. Environmental impact of fouling for crude oil flow in preheat pipes according to oil blends. *Heliyon* **2023**, *9*, e21999. [\[CrossRef\]](#)
7. Panchal, C.B.; Huangfu, E.P. Effects of mitigating fouling on the energy efficiency of crude-oil distillation. *Heat Transf. Eng.* **2000**, *21*, 3–9. [\[CrossRef\]](#)
8. Ishiyama, E.M.; Coletti, F.; Macchietto, S.; Paterson, W.R.; Wilson, D.I. Impact of deposit ageing on thermal fouling: Lumped parameter model. *AIChE J.* **2010**, *56*, 531–545. [\[CrossRef\]](#)
9. Coletti, F.; Ishiyama, E.M.; Paterson, W.R.; Wilson, D.I.; Macchietto, S. Impact of deposit aging and surface roughness on thermal fouling: Distributed model. *AIChE J.* **2010**, *56*, 3257–3273. [\[CrossRef\]](#)

10. Coletti, F.; Macchietto, S. A dynamic, distributed model of shell-and-tube heat exchangers undergoing crude oil fouling. *Ind. Eng. Chem. Res.* **2011**, *50*, 4515–4533. [\[CrossRef\]](#)
11. Ishiyama, E.M.; Paterson, W.R.; Ian Wilson, D. Exploration of alternative models for the aging of fouling deposits. *AIChE J.* **2011**, *57*, 3199–3209. [\[CrossRef\]](#)
12. Ishiyama, E.M.; Paterson, W.R.; Wilson, D.I. Aging is important: Closing the fouling-cleaning loop. *Heat Transf. Eng.* **2014**, *35*, 311–326. [\[CrossRef\]](#)
13. Diaz-Bejarano, E.; Behranvand, E.; Coletti, F.; Mozdianfard, M.R.; Macchietto, S. Organic and inorganic fouling in heat exchangers—Industrial case study: Analysis of fouling state. *Appl. Energy* **2017**, *206*, 1250–1266. [\[CrossRef\]](#)
14. Loyola-Fuentes, J.; Jobson, M.; Smith, R. Estimation of fouling model parameters for shell side and tube side of crude oil heat exchangers using data reconciliation and parameter estimation. *Ind. Eng. Chem. Res.* **2019**, *58*, 10418–10436. [\[CrossRef\]](#)
15. Diaz-Bejarano, E.; Coletti, F.; Macchietto, S. Modeling and Prediction of Shell-Side Fouling in Shell-and-Tube Heat Exchangers. *Heat Transf. Eng.* **2019**, *40*, 845–861. [\[CrossRef\]](#)
16. Georgiadis, M.C.; Rotstein, G.E.; Macchietto, S. Modeling and Simulation of Shell and Tube Heat Exchangers under Milk Fouling. *AIChE J.* **1998**, *44*, 959–971. [\[CrossRef\]](#)
17. Georgiadis, M.C.; Rotstein, G.E.; Macchietto, S. Optimal design and operation of heat exchangers under milk fouling. *AIChE J.* **1998**, *44*, 2099–2111. [\[CrossRef\]](#)
18. Aldi, N.; Casari, N.; Pinelli, M.; Suman, A.; Vulpio, A. Performance Degradation of a Shell-and-Tube Heat Exchanger Due to Tar Deposition. *Energies* **2022**, *15*, 1490. [\[CrossRef\]](#)
19. Romanowicz, T.; Taler, J.; Jaremkiwicz, M.; Sobota, T. Determination of Heat Transfer Correlations for Fluids Flowing through Plate Heat Exchangers Needed for Online Monitoring of District Heat Exchanger Fouling. *Energies* **2023**, *16*, 6264. [\[CrossRef\]](#)
20. Jradi, R.; Marvillet, C.; Jeday, M.R. Multi-objective optimization and performance assessment of response surface methodology (RSM), artificial neural network (ANN) and adaptive neuro-fuzzy interference system (ANFIS) for estimation of fouling in phosphoric acid/steam heat exchanger. *Appl. Therm. Eng.* **2024**, *248*, 123255. [\[CrossRef\]](#)
21. Ben-Mansour, R.; El-Ferik, S.; Al-Naser, M.; Qureshi, B.A.; Eltoum, M.A.M.; Abuelyamen, A.; Al-Sunni, F.; Ben Mansour, R. Experimental/Numerical Investigation and Prediction of Fouling in Multiphase Flow Heat Exchangers: A Review. *Energies* **2023**, *16*, 2812. [\[CrossRef\]](#)
22. Benzarti, Z.; Arrousse, N.; Serra, R.; Cruz, S.; Bastos, A.; Tedim, J.; Salgueiro, R.; Cavaleiro, A.; Carvalho, S. Copper corrosion mechanisms, influencing factors, and mitigation strategies for water circuits of heat exchangers: Critical review and current advances. *Corros. Rev.* **2024**. [\[CrossRef\]](#)
23. Assis, B.C.G.; Lemos, J.C.; Liporace, F.S.; Oliveira, S.G.; Queiroz, E.M.; Pessoa, F.L.P.; Costa, A.L.H. Dynamic Optimization of the Flow Rate Distribution in Heat Exchanger Networks for Fouling Mitigation. *Ind. Eng. Chem. Res.* **2015**, *54*, 6497–6507. [\[CrossRef\]](#)
24. Trafczynski, M.; Markowski, M.; Alabrudzinski, S.; Urbaniec, K. The influence of fouling on the dynamic behavior of PID-controlled heat exchangers. *Appl. Therm. Eng.* **2016**, *109*, 727–738. [\[CrossRef\]](#)
25. Rogel, E.; Hench, K.; Miao, T.; Lee, E.; Dickakian, G. Evaluation of the Compatibility of Crude Oil Blends and Its Impact on Fouling. *Energy Fuels* **2018**, *32*, 9233–9242. [\[CrossRef\]](#)
26. Rogel, E.; Hench, K.; Cibotti, F.; Forbes, E.; Jackowski, L. Investigation on Crude Oil Fouling Behavior. *Energy Fuels* **2022**, *36*, 818–825. [\[CrossRef\]](#)
27. Al Obaidi, Y.; Kozminski, M.; Ward, J.D. Method and Device for Quantitative Measurement of Crude Oil Fouling Deposits of Several Crude Oils and Blends at a Higher Temperature and the Impact of Antifoulant Additives. *Energy Fuels* **2018**, *32*, 6782–6787. [\[CrossRef\]](#)
28. M'barki, O.; Clements, J.; Nguyen, Q.P. Effects of Added Asphaltenes and Paraffin Inhibitor on Wax Stability and Deposition in Oils of Varying Complexity. *Energy Fuels* **2023**, *37*, 14790–14799. [\[CrossRef\]](#)
29. Villardi, H.G.D.; de Medeiros, F.F.; Orrico, L.C.; de Souza, A.L.B.; Junior, I.M.; Liporace, F.S.; Pessoa, F.L.P. Experimental Evaluation of the Deposition Dynamics of Different Petroleum Blends in a Benchtop Heat Exchanger Test Instrument. *Energies* **2023**, *16*, 7387. [\[CrossRef\]](#)
30. Lemos, J.C.; Costa, A.L.H.; Bagajewicz, M.J. Globally optimal linear approach to the design of heat exchangers using threshold fouling modeling. *AIChE J.* **2018**, *64*, 2089–2102. [\[CrossRef\]](#)
31. Lemos, J.C.; Costa, A.L.H.; Bagajewicz, M.J. Design of shell and tube heat exchangers considering the interaction of fouling and hydraulics. *AIChE J.* **2022**, *68*, e17586. [\[CrossRef\]](#)
32. Pan, M.; Bulatov, I.; Smith, R. Improving heat recovery in retrofitting heat exchanger networks with heat transfer intensification, pressure drop constraint and fouling mitigation. *Appl. Energy* **2016**, *161*, 611–626. [\[CrossRef\]](#)
33. de Carvalho, C.B.; de Carvalho, E.P.; Ravagnani, M.A.S.S. Optimization of Flow Rate Distribution in a Crude Oil Preheat Train Considering Fouling Deposition in Shell and Tube Sides. *Ind. Eng. Chem. Res.* **2022**, *61*, 5568–5577. [\[CrossRef\]](#)
34. Lozano-Santamaria, F.; Macchietto, S. Integration of optimal cleaning scheduling and control of heat exchanger networks under fouling: MPCC solution. *Comput. Chem. Eng.* **2019**, *126*, 128–146. [\[CrossRef\]](#)

35. Ishiyama, E.M.; Paterson, W.R.; Wilson, D.I. Platform for techno-economic analysis of fouling mitigation options in refinery preheat trains. *Energy Fuels* **2009**, *23*, 1323–1337. [[CrossRef](#)]
36. Pogiatis, T.; Ishiyama, E.M.; Paterson, W.R.; Vassiliadis, V.S.; Wilson, D.I. Identifying optimal cleaning cycles for heat exchangers subject to fouling and ageing. *Appl. Energy* **2012**, *89*, 60–66. [[CrossRef](#)]
37. Assis, B.C.G.; Lemos, J.C.; Queiroz, E.M.; Pessoa, F.L.P.; Liporace, F.S.; Oliveira, S.G.; Costa, A.L.H. Optimal allocation of cleanings in heat exchanger networks. *Appl. Therm. Eng.* **2013**, *58*, 605–614. [[CrossRef](#)]
38. Diaby, A.L.; Miklavcic, S.J.; Bari, S.; Addai-Mensah, J. Evaluation of crude oil heat exchanger network fouling behavior under aging conditions for scheduled cleaning. *Heat Transf. Eng.* **2016**, *37*, 1211–1230. [[CrossRef](#)]
39. Diaby, A.L.; Miklavcic, S.J.; Addai-Mensah, J. Optimization of scheduled cleaning of fouled heat exchanger network under ageing using genetic algorithm. *Chem. Eng. Res. Des.* **2016**, *113*, 223–240. [[CrossRef](#)]
40. Al Ismaili, R.; Lee, M.W.; Wilson, D.I.; Vassiliadis, V.S. Heat exchanger network cleaning scheduling: From optimal control to mixed-Integer decision making. *Comput. Chem. Eng.* **2018**, *111*, 1–15. [[CrossRef](#)]
41. Elwerfalli, A.; Alsadaie, S.; Mujtaba, I.M. Estimation of shutdown schedule to remove fouling layers of heat exchangers using risk-based inspection (RBI). *Processes* **2021**, *9*, 2177. [[CrossRef](#)]
42. Trafczynski, M.; Markowski, M.; Urbaniec, K. Energy saving and pollution reduction through optimal scheduling of cleaning actions in a heat exchanger network. *Renew. Sustain. Energy Rev.* **2023**, *173*, 113072. [[CrossRef](#)]
43. Trafczynski, M.; Markowski, M.; Urbaniec, K.; Trzcinski, P.; Alabrudzinski, S.; Suchecki, W. Estimation of thermal effects of fouling growth for application in the scheduling of heat exchangers cleaning. *Appl. Therm. Eng.* **2021**, *182*, 116103. [[CrossRef](#)]
44. Thulukkanam, K. *Heat Exchanger Design Handbook*; CRC Press: Boca Raton, FL, USA, 2013.
45. Lozano-Santamaria, F.; Macchietto, S. Integration of Optimal Cleaning Scheduling and Control of Heat Exchanger Networks Undergoing Fouling: Model and Formulation. *Ind. Eng. Chem. Res.* **2018**, *57*, 12842–12860. [[CrossRef](#)]
46. Offor, U.H.; Alabi, S.B. An Accurate and Computationally Efficient Explicit Friction Factor Model. *Adv. Chem. Eng. Sci.* **2016**, *6*, 237–245. [[CrossRef](#)]
47. Patil, P.; Srinivasan, B.; Srinivasan, R. Performance monitoring of heat exchanger networks using excess thermal and hydraulic loads. *Chem. Eng. Res. Des.* **2023**, *200*, 225–243. [[CrossRef](#)]
48. Lu, J.; Hu, H.; Bai, Y. Radial basis function neural network based on an improved exponential decreasing inertia weight-particle swarm optimization algorithm for AQI prediction. *Abstr. Appl. Anal.* **2014**, *2014*, 178313. [[CrossRef](#)]

Disclaimer/Publisher’s Note: The statements, opinions and data contained in all publications are solely those of the individual author(s) and contributor(s) and not of MDPI and/or the editor(s). MDPI and/or the editor(s) disclaim responsibility for any injury to people or property resulting from any ideas, methods, instructions or products referred to in the content.